Received: 27 February 2017 | Revised: 11 August 2017 | Accepted: 11 December 2017

DOI: 10.1002/stc.2139

RESEARCH ARTICLE

WILEY

Innovative substructure approach to estimating structural parameters of shear structures

Lijun Xie[1] | Akira Mita[1] | Longxi Luo[2] | Maria Q. Feng[2]

[1]Department of System Design Engineering, Keio University, Yokohama, Japan

[2]Department of Civil Engineering and Engineering Mechanics, Columbia University, New York, New York, USA

Correspondence
Lijun Xie, Department of System Design Engineering, Keio University, 14-620D, Mita Laboratory, 3-14-1 Hiyoshi, Kohoku-ku, Yokohama, Japan 223-8522.
Email: dierxie@keio.jp; dier_xie@163.com

Summary

An innovative substructure approach is proposed for estimating the structural parameters of shear structures from the acceleration responses of individual substructures. Two parallel methods are created to form single-degree-of-freedom models of each substructure. The behavioral characteristics of these substructure models chiefly depend on the structural parameters of the edges of the component substructure, which is separate from the shear structure. To obtain structural parameters from the substructure accelerations, discrete substructure models with accelerations are generated using Newmark's method and are found similar to the autoregressive moving average with exogenous (ARMAX) inputs models. Sophisticated techniques for solving ARMAX models are used to process the accelerations and to extract the structural parameters of the substructures. A linear relationship among model coefficients of the discrete substructure models and ARMAX models is discovered that provides an accurate and simple way to identify all the substructure parameters. A numerical simulation of a 10-story shear structure during earthquake is performed to verify this substructure approach, where the factors of the size of the substructure and the noise disturbance are considered. Finally, this substructure approach is used to identify a structural model and reproduce the structural responses of a five-story three-dimensional structure in a shaking-table experiment.

KEYWORDS

ARMAX model, shaking-table experiment, shear structure, structural parameter identification, substructure approach

1 | INTRODUCTION

Structural health monitoring (SHM) has advantages of objective and nondestructive detection and has been widely studied by engineers and researchers in civil engineering as a way of keeping track of damage to structures and assessing their structural integrity in terms of safety and reliability.[1] Determining the dynamic characteristics and model parameters of complex structural systems is the primary concern in SHM for model updating, active control, damage detection, and prognosis.[2,3] The tremendous quantity of unknown parameters and large number of incomplete measurements make SHM a significant challenge on large structures such as tall buildings and bridges. Appropriately extracted structural characteristics associated with a suitably designed monitoring strategy are especially vital for ensuring the effectiveness and feasibility of any SHM system.

Modal parameters such as the natural frequency, damping ratio, and mode shape play an important role in establishing and updating appropriate structural models[4] in SHM. However, modal parameters are not very sensitive to variations in local structural properties, especially in huge structures.[5] A common belief among researchers is that modal parameters are reflections of the entire structure, whereas physical parameters such as mass, stiffness, and damping reflect the local structural properties. Furthermore, it is quite difficult to identify all the modal information or accurately infer structural physical parameters from incomplete sets of modal parameters. The large number of unknown parameters also hinders any effort aimed at improving identification efficiency and robustness.

The substructure approach may be a way to overcome the above obstacles in structural parameter identification by separately estimating the structural physical parameters. By cutting the whole structure into several parts, the properties and characteristics of each part can be independently identified. Because the idea was probably first proposed by Koh et al.,[6] a variety of substructure approaches have been presented for structural parameter identification and damage identification in buildings and bridges and have been verified in numerical simulations. These include the substructure approaches only using accelerations[7] or under the condition without measurement on the interface of the beam structure,[8] the Bayesian frequency-domain substructure approach using noisy measurements,[9] the substructure approach with incomplete measurement,[10] the isolated substructure approach by placing virtual supports on the interfaces of the substructure,[11,12] the substructure approach in the frequency domain for shear structures using cross-power spectral densities,[13] and others.

The major concern of the substructure approaches is dealing with the interaction forces at interface of the isolated substructure and the performance of the substructure approaches in the primary stage of development mostly relied on the use of iterative algorithms to estimate the unknown physical parameters. For example, the algorithms that operate in the time domain include the extended Kalman filtering,[6,14] the genetic algorithm,[7,8] the observer/Kalman filter identification and the Eigen system realization algorithm,[10,15] and the sequential prediction error method.[16] The algorithms in the frequency domain include modified successive linear programming.[17] With the continued development of computer science and related techniques, many of these iterative algorithms can now be executed on practical computational platforms. Some researchers have since switched their attention to the substructure approaches.

Mita[18] described a distributed health monitoring system equipped with accelerometers that can preliminarily process vibration data of pipeline architecture that can be modeled as shear structure. Xing and Mita[19] and Mei et al.[20] developed the distributed health monitoring system into substructures by taking out one floor from a tall building to form a single-degree-of-freedom (SDOF) system and to detect structural damage inside the substructure. This approach is very efficient as it only needs to process three accelerations each time and is very easy for engineers to use. Instead of developing complex algorithms, the autoregressive-moving average with exogenous (ARMAX) model, a sophisticated statistic model that has been incorporated in many software platforms, can be used to process the accelerations. However, because structural parameter identification is not the focus in the above research, the structural parameters of different parts of the structure are still mixed together. In that research, it was almost impossible to separately obtain individual structural parameters from a substructure.

This paper describes an innovative substructure approach that makes it possible to conduct a parallel structural parameter identification of every substructure. It is based on the research of Xing and Mita[19] and Mei et al.[20] But different from the previous substructure approaches where all unknown parameters of the edges and inner part of the substructure are treated equally, the proposed approach only focuses on identifying the parameters of the edges of the substructure. In so doing, the ability to deal with different substructures is obviously improved, whereas the number of unknown parameters in the calculation is greatly reduced.

Three steps are proposed to realize the innovative substructure approach: structure separation, model discreteness, and data processing. First, any part of a shear structure can be separated into very fine SDOF substructure models by rearranging the structural parameters in the corresponding equations of motion. The structural parameters of the edges (upper and lower edges of a building) of the substructure are the major parameters in these models. Second, substructure models with accelerations are formulated on the basis of Newmark's method in a discrete time space. These discrete substructure models, after taking into account error terms, are equal in performance to ARMAX models. Third, the techniques for solving ARMAX models are used to process acceleration measurements and extract the structural parameters. The coefficients of the ARMAX model are functions of the structural parameters in the substructure model. A linear relationship among the coefficients of the ARMAX model can be easily revealed and can be used to estimate all the unknown structural parameters of a substructure.

The parameters of the whole structure can then be estimated through a parallel calculation of the substructures. Moreover, the behavior of critical parts of the shear structure can be individually monitored in the substructures. The

substructure identification strategy with overlapping (where the substructures overlap and share some parts of the structure) is used to estimate the structural parameters of the whole structure. The performance of the structural identification can be judged by comparing the simulated accelerations of the identified structural model with the measured accelerations of the real structure.

Numerical simulations of a 10-story shear building subject to earthquake vibrations were conducted to verify the performance of the new substructure approach. Substructures of various sizes and two kinds of noise disturbances were simulated. In addition, the new substructure approach was compared with previous research.[19,20] Finally, a shaking-table experiment of a five-story three-dimensional frame was carried out to test the efficiency of the approach. The percent errors of the identified structural parameters with theoretical values were calculated and the simulated and measured accelerations were compared in order to examine the accuracy of the structural parameter identification.

This paper is organized as follows. Section 2 describes the derivation of the proposed substructure approach. Section 3 shows the numerical simulation of a 10-story building subjected to earthquake vibration. Section 4 describes the experiment on a five-story three-dimensional frame. Section 5 is the conclusion.

2 | NEW SUBSTRUCTURE APPROACH FOR PARAMETER IDENTIFICATION

The shear structure model is a lumped mass in the shape of a building whose basement is subjected to lateral vibrations, as shown in Figure 1a. The number of stories in the building is n. The equations of motion of the whole structure can be described as

$$\mathbf{M}\ddot{\mathbf{z}}(t) + \mathbf{C}\dot{\mathbf{z}}(t) + \mathbf{K}\mathbf{z}(t) = -\mathbf{M}\mathbf{L}\ddot{x}_g(t), \tag{1}$$

where $(\cdot)$ denotes the time derivative, $\ddot{x}_g(t)$ the acceleration of the basement, and $\mathbf{z}(t)$ the displacement vector of the structure relative to the basement; $\mathbf{M}$, $\mathbf{C}$, and $\mathbf{K}$ are the structural mass, damping and stiffness matrixes, respectively, whereas $\mathbf{L}$ is an $n \times 1$ unit vector ($\mathbf{L} = [1\cdots1]^T$).

Now, let us consider a substructure that includes stories running from the ith to the $(i + l)^{th}$ ($l > 0$, the number of internal degrees of freedom [DOFs]), as shown in Figure 1b. This substructure is denoted as Sub.#(i, $i + l$), where i and $i + l$ are the story numbers on the edges of the substructure. There are two methods of forming substructure models for the building.

Method 1 is as follows. The equations of motion of the internal DOFs of Sub.#(i, $i + l$) can be written as

$$m_j\ddot{x}_j(t) + c_j\dot{y}_j(t) - c_{j+1}\dot{y}_{j+1}(t) + k_j y_j(t) - k_{j+1}y_{j+1}(t) = 0, \quad j = i, ..., i + l - 1. \tag{2}$$

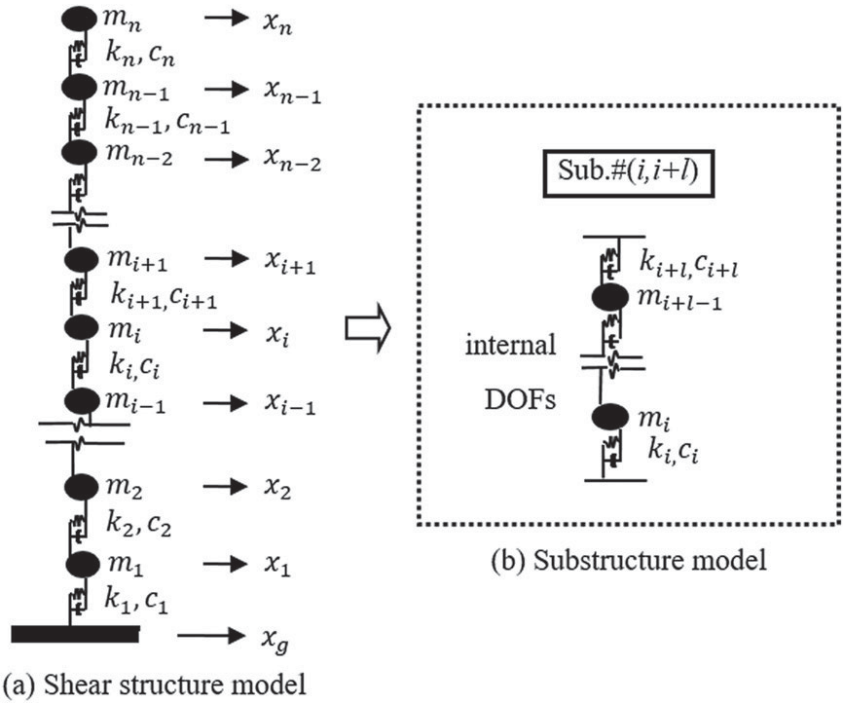

FIGURE 1 Division of shear structure model of a building

where $x_j(t)$ and $y_j(t)$ are respectively the absolute movement and inter-story deformation (or drift) of the jth story, calculated as below:

$$x_j(t) = z_j(t) + x_g(t), \tag{3}$$

$$y_j(t) = z_j(t) - z_{j-1}(t). \tag{4}$$

The sum of the series of Equation 2 is

$$\sum_{j=i}^{i+l-1} m_j\ddot{x}_j(t) + c_i\dot{y}_i(t) + k_i y_i(t) - c_{i+l}\dot{y}_{i+l}(t) - k_{i+l}y_{i+l}(t) = 0. \tag{5}$$

Equation 5 can be arranged by adding $l(m_i\ddot{y}_i(t) - m_i\ddot{y}_i(t) = 0)$ to it, as follows:

$$\ddot{y}_i(t) + \frac{c_i}{lm_i}\dot{y}_i(t) + \frac{k_i}{lm_i}y_i(t) = \ddot{X}_I(t) + \frac{c_{i+l}}{lm_i}\dot{y}_{i+l}(t) + \frac{k_{i+l}}{lm_i}y_{i+l}(t), \tag{6}$$

where

$$\ddot{X}_I(t) = -\sum_{j=i}^{i+l-1}\frac{m_j}{lm_i}\ddot{x}_j(t) + \ddot{y}_i(t). \tag{7}$$

Viewing the right side of the equation as input, Equation 6 is the SDOF substructure model in Method 1. $\ddot{X}_I(t)$ is the sum of accelerations of the substructure. Usually, $i = 1, ..., n$; $l = 1, ..., n - i + 1$. Moreover, if $(i + l) > n$, imaginary stories from the $(n + 1)^{\text{th}}$ to $(i + l)^{\text{th}}$ with no physical meaning or dynamic vibrations can be constructed on the top of the building to keep Equation 6 balanced for Sub.#(i, $i + l$).

Newmark's method from 1959[21] converts displacements and velocities into accelerations in a discrete time space:

$$x(t) - 2x(t-1) + x(t-2) = \alpha\Delta t^2\ddot{x}(t) + (0.5 - 2\alpha + \delta)\Delta t^2\ddot{x}(t-1) + (0.5 + \alpha - \delta)\Delta t^2\ddot{x}(t-2), \tag{8}$$

$$\dot{x}(t) - 2\dot{x}(t-1) + \dot{x}(t-2) = \delta\Delta t\ddot{x}(t) + (1-2\delta)\Delta t\ddot{x}(t-1) - (1-\delta)\Delta t\ddot{x}(t-2), \tag{9}$$

where $0 \le \delta \le 1$ and $0 \le \alpha \le 0.5$ are parameters, and Δt is the sampling period, which is assumed to be constant. Organizing Equation 6 at sampling time t, $t - 1$, and $t - 2$ as the left side of Equation 8 or 9 and substituting Equations 8 and 9 to it yield a discrete substructure model including only accelerations:

$$\begin{aligned}[1 + \Theta_1(m_i, c_i, k_i)]\ddot{y}_i(t) + [-2 + \Theta_2(m_i, c_i, k_i)]\ddot{y}_i(t-1) + [1 + \Theta_3(m_i, c_i, k_i)]\ddot{y}_i(t-2)\\ = \ddot{X}_I(t) - 2\ddot{X}_I(t-1) + \ddot{X}_I(t-2) + \Theta_1(m_i, c_{i+l}, k_{i+l})\ddot{y}_{i+l}(t)\\ + \Theta_2(m_i, c_{i+l}, k_{i+l})\ddot{y}_{i+l}(t-1) + \Theta_3(m_i, c_{i+l}, k_{i+l})\ddot{y}_{i+l}(t-2),\end{aligned} \tag{10}$$

where $\Theta_1(.)$, $\Theta_2(.)$ and $\Theta_3(.)$ are functions defined as

$$\Theta_1(m, c, k) = \delta\Delta t\frac{c}{lm} + \alpha\Delta t^2\frac{k}{lm}, \tag{11}$$

$$\Theta_2(m, c, k) = (1-2\delta)\Delta t\frac{c}{lm} + (0.5 - 2\alpha + \delta)\Delta t^2\frac{k}{lm}, \tag{12}$$

$$\Theta_3(m, c, k) = -(1-\delta)\Delta t\frac{c}{lm} + (0.5 + \alpha - \delta)\Delta t^2\frac{k}{lm}. \tag{13}$$

By taking model errors into account in Equation 10, the discrete substructure model of Sub.#(i, $i + l$) can then be transformed into an ARMAX model, a sophisticated statistic model that is included in a number of software products:

$$\begin{aligned}\ddot{y}_i(t) + a_1(m_i, c_i, k_i)\ddot{y}_i(t-1) + a_2(m_i, c_i, k_i)\ddot{y}_i(t-2) = b_{11}(m_i, c_i, k_i)\ddot{X}_I^c(t) + b_{21}(m_i, c_i, k_i, c_{i+l}, k_{i+l})\ddot{y}_{i+l}(t)\\ + b_{22}(m_i, c_i, k_i, c_{i+l}, k_{i+l})\ddot{y}_{i+l}(t-1) + b_{23}(m_i, c_i, k_i, c_{i+l}, k_{i+l})\ddot{y}_{i+l}(t-2) + e(t) + g_1e(t-1) + g_2e(t-2),\end{aligned} \tag{14}$$

where

$$\ddot{X}_I^c(t) = \ddot{X}_I(t) - 2\ddot{X}_I(t-1) + \ddot{X}_I(t-2), \tag{15}$$

$\ddot{X}_I^c(t)$ is pre-calculated, $e(t)$ is the model residuals, and $a_1(.)$, $a_2(.)$, $b_{11}(.)$, $b_{21}(.)$, $b_{22}(.)$, $b_{23}(.)$, g_1 and g_2 are the estimated model coefficients. There are two moving-average terms ($e(t-1)$, $e(t-2)$) in the ARMAX model. From simulation analysis, when the number of moving-average terms equal to or bigger than two, the model is robust against the noise and the number of moving-average terms does not make a big difference. The correspondences between the coefficients of the ARMAX model and that of Equation 10 are presented in Table 1, where $\Theta_1(.)$, $\Theta_2(.)$, and $\Theta_3(.)$ are as in Equations 11 to 13.

The denominators in Table 1 become 1 in the special case of Newmark's method ($\delta = 0$, $\alpha = 0$), $\Theta_1(.) = 0$ (Equation 11), and $b_{21}(\cdot) = 0$. In this case, replacing the physical parameters (c_i, k_i) in the expressions of $a_1(\cdot)$ and $a_2(\cdot)$ with (c_{i+l}, k_{i+l}) leads to the following linear relationship between $b_{22}(\cdot)$, $b_{23}(\cdot)$, and $a_1(\cdot)$, $a_2(\cdot)$:

$$\begin{aligned} a_1(m_i, c_{i+l}, k_{i+l}) &= b_{22}(m_i, c_{i+l}, k_{i+l}) - 2, \\ a_2(m_i, c_{i+l}, k_{i+l}) &= b_{23}(m_i, c_{i+l}, k_{i+l}) + 1. \end{aligned} \tag{16}$$

This linear relationship also appears in Equation 10. The ARMAX model (Equation 14) in the above special case of Newmark's method becomes more condensed and can be used for parameter identification.

The structural parameters of the substructure model (Equation 6) can be identified by examining the coefficients of the ARMAX model (Equation 14) on the basis of the relation between Laplace-transform and Z-transform, which has been studied in the theory of experimental modal analysis and has been utilized in Lee and Yun[22] to estimating structural modal quantities such as natural frequencies, damping ratios, and mode shapes from the measurements. The process for identifying the structural stiffness from the ARMAX model of the related substructure is demonstrated as follows.

The Laplace-transform of Equation 6, that is, the continuous substructure model of Sub.#(i, $i+l$), can be written as below:

$$Y_i(s) = \frac{s^2 \mathcal{L}\left\{\ddot{X}_I(t) + \frac{c_{i+l}}{lm_i}\dot{y}_{i+l}(t) + \frac{k_{i+l}}{lm_i}y_{i+l}(t)\right\}}{s^2 + \frac{c_i}{lm_i}s + \frac{k_i}{lm_i}} = \frac{s^2 \mathcal{L}\{U(t)\}}{(s-\lambda_s)(s-\lambda_s^*)}, \tag{17}$$

where $\mathcal{L}\{\cdot\}$ is the denotation of Laplace-transform, $Y_i(s) = \mathcal{L}\{\ddot{y}_i(t)\}$ the Laplace-transform of $\ddot{y}_i(t)$, and (λ_s, λ_s^*) the poles of the system, which are related with structural parameters,

$$\lambda_s, \lambda_s^* = -\frac{1}{2}\frac{c_i}{lm_i} \pm \sqrt{\frac{1}{4}\left(\frac{c_i}{lm_i}\right)^2 - \frac{k_i}{lm_i}}. \tag{18}$$

The (λ_s, λ_s^*) are complex numbers. Equation 18 builds a relationship between k_i and (λ_s, λ_s^*), given as below:

$$k_i = lm_i(\lambda_s \cdot \lambda_s^*) = lm_i|\lambda_s|^2. \tag{19}$$

In parallel, the Z-transform of Equation 14, that is, the ARMAX model of Sub.#(i, $i+l$), can be written as

$$Y_i(Z) = \frac{\mathcal{Z}\{U'(t)\}}{1 + a_1(m_i, c_i, k_i)Z^{-1} + a_2(m_i, c_i, k_i)Z^{-2}} = \frac{Z^2 \cdot \mathcal{Z}\{U'(t)\}}{(Z-\lambda_Z)(Z-\lambda_Z^*)}, \tag{20}$$

TABLE 1 Expressions for the coefficients of ARMAX model with structural parameters

ARMAX Model	$a_1(.)$	$a_2(.)$	$b_{11}(.)$	$b_{21}(.)$	$b_{22}(.)$	$b_{23}(.)$
Equation 14	$\frac{-2+\Theta_2(m_i,c_i,k_i)}{1+\Theta_1(m_i,c_i,k_i)}$	$\frac{1+\Theta_3(m_i,c_i,k_i)}{1+\Theta_1(m_i,c_i,k_i)}$	$\frac{1}{1+\Theta_{1(m_i,c_i,k_i)}}$	$\frac{\Theta_1(m_i,c_{i+l},k_{i+l})}{1+\Theta_1(m_i,c_i,k_i)}$	$\frac{\Theta_2(m_i,c_{i+l},k_{i+l})}{1+\Theta_1(m_i,c_i,k_i)}$	$\frac{\Theta_3(m_i,c_{i+l},k_{i+l})}{1+\Theta_1(m_i,c_i,k_i)}$

Note. ARMAX = autoregressive-moving average with exogenous.

where $U^{'}(t)$ is the part on the right side of Equation 14; $\mathcal{Z}\{\cdot\}$ denotes Z-transform; $Y_i(Z) = \mathcal{Z}\{\ddot{y}_i(t)\}$ is the Z-transform of $\ddot{y}_i(t)$ where t is the discrete time; (λ_Z, λ_Z^*) are the poles of the system. Defining $Z = e^{s\Delta t}$, the Z-transform $Y_i(Z)$, becomes proportional to the Laplace-transform $Y_i(s)$. Correspondingly, the poles (λ_Z, λ_Z^*) and (λ_s, λ_s^*) has relations as below:

$$\lambda_Z = e^{\lambda_s \Delta t} \text{ or } \lambda_Z^* = e^{\lambda_s^* \Delta t}, \text{ i.e. } \lambda_s = \frac{\ln(\lambda_Z)}{\Delta t} \text{ or } \lambda_s^* = \frac{\ln(\lambda_Z^*)}{\Delta t}. \tag{21}$$

Submitting Equation 21 into Equation 19, the k_i can be expressed by λ_Z, as seen below:

$$k_i = lm_i \left(\frac{|\ln(\lambda_Z)|}{\Delta t} \right)^2. \tag{22}$$

Assuming the structural mass is already known, ${}_1\widetilde{k}^{i|(i,i+l)}$ and ${}_1\widetilde{k}^{i+l|(i,i+l)}$ are the corresponding estimates of k_i and k_{i+l} in Sub.#$(i, i+l)$. Based on Equation 22, ${}_1\widetilde{k}^{i|(i,i+l)}$ is calculated as

$${}_1\widetilde{k}_{i|(i,i+l)} = lm_i \left(\frac{|\ln \mu a|}{\Delta t} \right)^2, \tag{23}$$

where μa or μa^* is the null point of an equation formed by the coefficients of the ARMAX model (Equation 14), as shown below:

$$1 + a_1(m_i, c_i, k_i)\mu a^{-1} + a_2(m_i, c_i, k_i)\mu a^{-2} = 0. \tag{24}$$

Because the coefficients $(a_1(\cdot), a_2(\cdot))$ are functions of $(b_{22}(\cdot), b_{23}(\cdot))$, as illustrated in Equation 16, ${}_1\widetilde{k}^{i+l|(i,i+l)}$ can be obtained by substituting Equation 16 into Equation 24 and solving for the null point μb or μb^*:

$${}_1\widetilde{k}^{i+l|(i,i+l)} = lm_i \left(\frac{|\ln \mu b|}{\Delta t} \right)^2. \tag{25}$$

Method 2 is as follows. Analogously, the structural parameters k_i and k_{i+l} in Sub.#$(i, i+l)$ can be obtained by using Method 2, wherein the substructure model is formed by adding $l\left(m_{i+l-1}\ddot{y}_{i+l}(t) - m_{i+l-1}\ddot{y}_{i+l}(t) = 0\right)$ to Equation 5:

$$\ddot{y}_{i+l}(t) + \frac{c_{i+l}}{lm_{i+l-1}}\dot{y}_{i+l}(t) + \frac{k_{i+l}}{lm_{i+l-1}}y_{i+l}(t) = \ddot{X}_I^{'}(t) + \frac{c_i}{lm_{i+l-1}}\dot{y}_i(t) + \frac{k_i}{lm_{i+l-1}}y_i(t). \tag{26}$$

where

$$\ddot{X}_I^{'}(t) = \sum_{j=i}^{i+l-1} \frac{m_j}{lm_{i+l-1}}\ddot{x}_i(t) + \ddot{y}_{i+l}(t). \tag{27}$$

Similar to Equation 6 in Method 1, Equation 26 can also be transformed into an ARMAX model by using the procedure described above. Accordingly, ${}_2\widetilde{k}^{i+l|(i,i+l)}$ and ${}_2\widetilde{k}^{i|(i,i+l)}$, that is, the estimates of k_{i+l} and k_i in Sub.#$(i, i+l)$ in Method 2, can be obtained from the coefficients of the ARMAX model:

$${}_2\widetilde{k}^{i+l|(i,i+l)} = lm_{i+l-1} \left(\frac{|\ln \mu a^{'}|}{\Delta t} \right)^2, \tag{28}$$

$${}_2\widetilde{k}^{i|(i,i+l)} = lm_{i+l-1} \left(\frac{|\ln \mu b^{'}|}{\Delta t} \right)^2, \tag{29}$$

where $\mu a^{'}$ and $\mu b^{'}$ are respectively the roots of the equations formed from $(1, a_1(\cdot), a_2(\cdot))$ and $(1, b_{22}(\cdot) - 2, b_{23}(\cdot) + 1)$ of the ARMAX model of Method 2. The $\ddot{y}_{n+1}(t)$ is a pseudo acceleration of $(n+1)^{\text{th}}$ story relative to nth story. Because there are

only n stories in the structure, $\ddot{y}_{n+1}(t) = 0$. Note when $\ddot{y}_{n+1}(t) = 0$, Method 1 still works whereas Method 2 can no longer be applied. Because $\ddot{y}_{i+l}(t)$ is the output of the system in Method 2, Method 2 cannot work if $\ddot{y}_{i+l}(t) = 0$. Therefore, Method 2 works for Sub #(i, $i + l$) with $i + l < n + 1$.

The major difference between Method 1 and Method 2 is that part of the model input and output information are interchanged. Hence, either method can be used to obtain the structural parameters of a specific story of a building from a substructure containing that story as one of its edges. In addition, for a specific ith story ($1 < i \leq n$), it can appear as the upper edge or the lower edge of the substructure used in the identification; that is, k_i ($1 < i \leq n$) can be estimated from Sub.#(i-l, i) ($1 \leq l < i$), where the ith story is the upper edge, or from Sub.#(i, $i + l$) ($0 < l \leq n$-$i + 1$), where the ith story is the lower edge. Both methods can be used to calculate k_i from those two substructure types. Table 2 lists the various representatives of k_i.

The proposed substructure approach can separately and independently estimate the stiffness of different edges of a substructure by using either Method 1 or Method 2. All the structural stiffness can be identified by appropriately dividing the shear structure into substructures. The only measurements that have to be made are of the acceleration responses of the substructures. The ARMAX models only need the ratio between the masses of different floors. The approach does not require detailed information about the masses for the calculation of the relative variation in stiffness or for the structural finite element model normalized by the mass.

This approach is intended to be used for small earthquake so that the structure vibrates within linear range and the nonlinearity does not pose major problems in the structural identification. Of course, during the major earthquake with large magnitude, the nonlinear response should be considered if this method is applied. This approach can be used under

TABLE 2 Various stiffness identifications for a specific story of a building

Representative value	Sub.#(i-l, i)		Sub.#(i, $i + l$)	
	Method 1	Method 2	Method 1	Method 2
$\widetilde{k}_i$	${}_1\widetilde{k}^{i\|(i-l,i)}$	${}_2\widetilde{k}^{i\|(i-l,i)}$	${}_1\widetilde{k}^{i\|(i,i+l)}$	${}_2\widetilde{k}^{i\|(i,i+l)}$

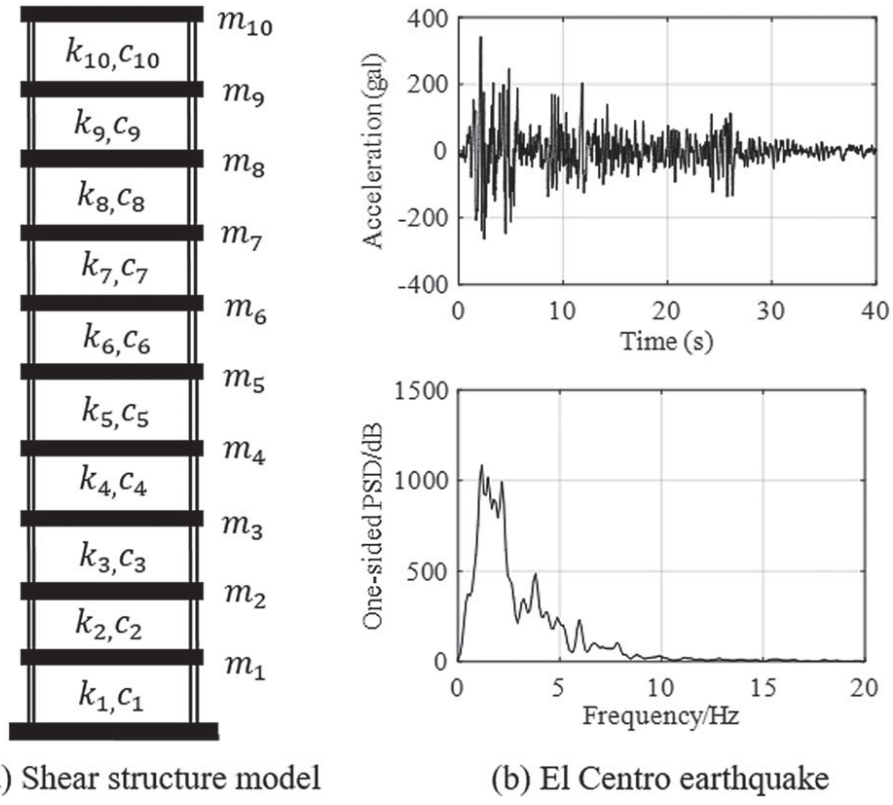

FIGURE 2 Shear structure model of a 10-story building

less severe vibration before and after the large earthquake to check if the structure suffers permanent damage. For small vibration, the response can be considered linear.

3 | NUMERICAL SIMULATION

The capabilities of the substructure approach were assessed in a simulation in which vibrations were applied to the basement of a 10-story building. The acceleration responses of the structure were generated using the state-space method. The shear structure model of the building is shown in Figure 2a. The masses of the floors were equal (1,000 tons). The lateral stiffness of each floor decreased from 2.00×10^6 kN/m to 1.64×10^6 kN/m as the floor height increased. The structure suffered stiffness proportional damping; this was simulated by defining the first-order global damping ratio as 0.005. The first three-orders of the global natural frequencies were 1.03, 3.02, and 4.96 Hz, and the first three-orders of the global damping ratio were 0.005, 0.015, and 0.024.

The 1940 El Centro earthquake (N-S acceleration) data were used as the input to the structure. The sampling frequency was 100 Hz. The time history and power spectral density of the quake are illustrated in Figure 2b, which shows that the major components are frequencies less than 5 Hz, near the lower-order frequencies of the building.

The environmental disturbances in the measured $\ddot{\tilde{x}}_i(t)$ were modeled as Gaussian white noise, $\ddot{w}_i(t) \sim N(0, \sigma_i^2)$. $\ddot{\tilde{x}}_i(t) = \ddot{x}_i(t) + \ddot{w}_i(t), i = 1, .., 10$, where $\ddot{x}_i(t)$ is the unpolluted data. The noise level R was characterized by the ratio of its root-mean-square (rms), that is, σ_i, to either the rms of $\ddot{z}_i(t)$ (the first noise scenario) or the rms of the basement vibration $\ddot{x}_g(t)$ (the second noise scenario). In the first noise scenario, the noise intensity or σ_i varied with the position of the floors, and the higher floors usually had larger noise intensities. In the second noise scenario, the noise intensity or σ_i was the same for every floor.

3.1 | Effect of varying the size of the substructure

Theoretically, a substructure can be an arbitrary continued part of the structure. However, the more floors there are in a substructure, the more accelerometers are needed, and the larger the cost of the local monitoring system becomes in turn.

Denoting *num_f* as the size of the substructure, *num_f* is defined as the number of DOFs (or floors including the basement of the building) in the substructure. For Sub.#(i, $i + l$), *num_f* is calculated as

$$num_f = l + 2 \ (l = 1, \ \ldots, \ n{-}i + 1; i = 1, \ \ldots, \ n). \tag{30}$$

Correspondingly, the number of accelerometers required for the substructure is

$$na = \min(i + l, n){-}i + 2. \tag{31}$$

where $num\_f \in [3, n + 2]$, $na \in [2, n + 1]$. Figure 3 shows the ranges of *num_f* and *na* for substructures at different positions of the 10-story building. The figures show that *na*=*num_f* for most of the substructures, except for those separated at the imaginary floor (the 11th floor here), where $na = num\_f - 1$. For example, $num\_f = 3$ and $na = 2$ are for the substructure at $i = 10$ in Figure 3. The substructures at $i = 9$ with $num\_f = 3$ or 4 share the same *na* (=3).

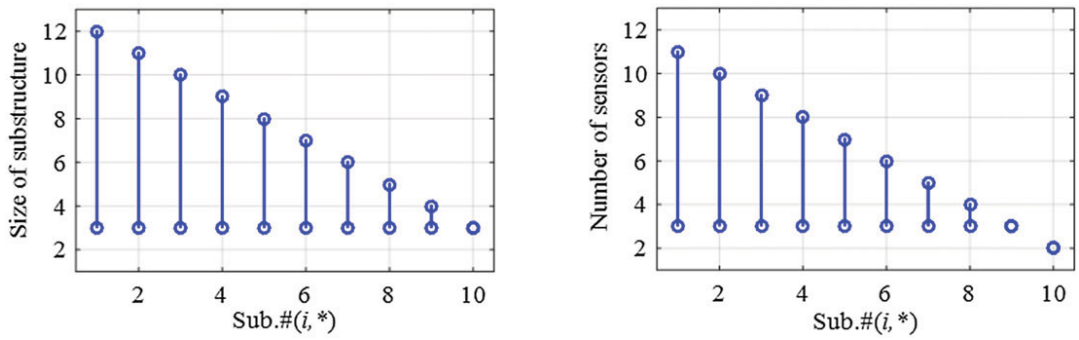

FIGURE 3 Ranges of *num_f* (left) and *na* (right) for substructures at different positions

Now considering substructures with different sizes at $i = 1$ (first story), that is, Sub.#(1, 1 + l) (l = 1, ..., 10; num_f = 3, ..., 12), four stiffness estimations ($\left({}_1\widetilde{k}_{1|(1,1+l)},\ {}_1\widetilde{k}_{1+l|(1,1+l)},{}_2\widetilde{k}_{1|(1,1+l)},{}_2\widetilde{k}_{1+l|(1,1+l)}\right)$, defined as Equations 23, 25, 29, and 28, can be obtained by using Methods 1 and 2 to represent k_1 and k_{1+l} in the substructures. The exception is Sub.#(1,11) with $l = 10$, where only ${}_1\widetilde{k}^{1|(1,\ 11)}$ can be estimated. The percent error is used to represent the identification accuracy. For example, the percent error of ${}_1\widetilde{k}_{1|(1,\ 11)}$ (see Equation 23) is

$$error\_{}_1\widetilde{k}_{i|(i,i+l)} = \frac{\left|{}_1\widetilde{k}_{i|(i,i+l)} - k_i\right|}{k_i}\ 100. \tag{32}$$

Figures 4–6 plot the percent errors of $\left({}_1\widetilde{k}_{1|(1,\ 1+l)},{}_1\widetilde{k}_{1+l|(1,\ 1+l)}\right)$ of Method 1 and $\left({}_2\widetilde{k}^{1|(1,\ 1+l)},{}_2\widetilde{k}^{1+l|(1,\ 1+l)}\right)$, of Method 2 with l = 1, ..., 10 for accelerations without noise and with 5% and 10% noise in the first noise scenario. The stiffness estimations of Method 1 are very close to those of Method 2 at the same level of noise. The majority of the percent errors of the stiffness estimates of Method 1 are ≤2% (no noise), ≤7% (5% noise), and ≤18% (10% noise), and the majority of those of Method 2 are ≤1.5% (no noise), ≤7.5% (5% noise), and ≤15% (10% noise).

The percent errors of the estimates for k_1 (${}_1\widetilde{k}^{1|(1,\ 1+l)}$ and ${}_2\widetilde{k}^{1|(1,\ 1+l)}$), the blue bars in Figures 4–6, decrease as l increases, whereas the percent errors of the estimates for k_{1+l} (${}_1\widetilde{k}^{1+l|(1,\ 1+l)}$ and ${}_2\widetilde{k}^{1+l|(1,\ 1+l)}$), the green bars in Figures 4–6, initially decrease before starting to climb. The transition points of the percent errors of (${}_1\widetilde{k}^{1+l|(1,\ 1+l)}$ and ${}_2\widetilde{k}^{1+l|(1,\ 1+l)}$) shift to smaller l as the noise level increases. At 10% noise, the transition points are very close to $l = 2$. Thus, $l = 2$ can be determined for Sub.#(i, $i + l$) ($i \le n - l$), whereas the substructures at $i > n - l$ can be determined as Sub.#(i, $n + 1$). The size of the substructure is $num\_f = 4$, and the number of accelerometers is $na = 4$ for Sub.#(i, $i + 2$) ($i \le n - 2$).

3.2 | System parameter identification of the whole building

The above discussion suggests that a shear structure can be partitioned into substructures containing four floors (including imaginary floors and basement). Because i is the only variation in Sub.#(i, $i + 2$) ($i \le n - 2$) or Sub.#(i, $n + 1$)

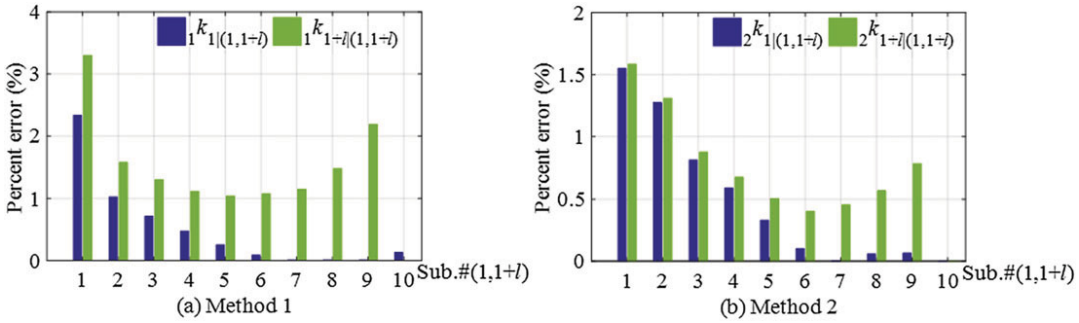

FIGURE 4 Percent error of estimates $\left({}_1\widetilde{k}^{1|(1,\ 1+l)},{}_1\widetilde{k}^{1+l|(1,\ 1+l)},{}_2\widetilde{k}^{1|(1,\ 1+l)},{}_2\widetilde{k}^{1+l|(1,\ 1+l)}\right)$ of Sub. # (1, 1 + l) (l = 1, ..., 10) (no noise)

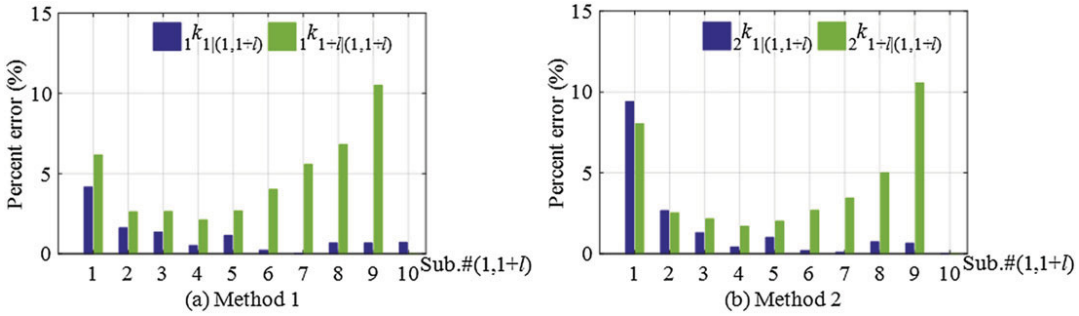

FIGURE 5 Percent error of estimates $\left({}_1\widetilde{k}^{1|(1,\ 1+l)},{}_1\widetilde{k}^{1+l|(1,\ 1+l)},{}_2\widetilde{k}^{1|(1,\ 1+l)},{}_2\widetilde{k}^{1+l|(1,\ 1+l)}\right)$ of Sub. # (1, 1 + l) (l = 1, .., 10) (5% noise in the first noise scenario)

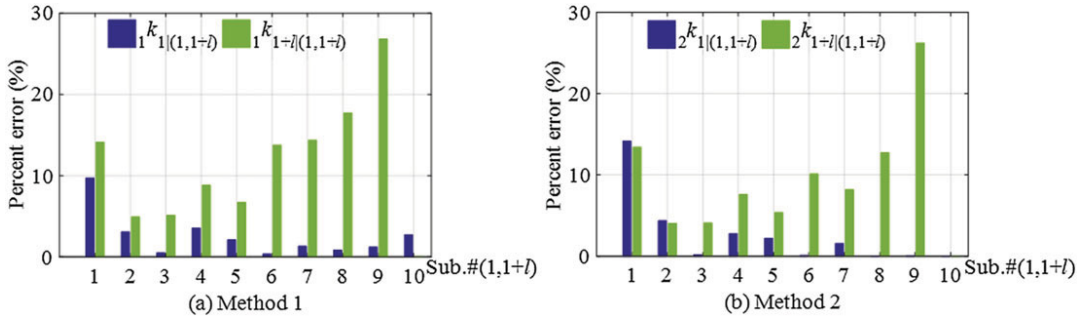

FIGURE 6 Percent error of estimates $\left({}_1\tilde{k}^{1|(1,\ 1+l)}, {}_1\tilde{k}^{1+l|(1,\ 1+l)}, {}_2\tilde{k}^{1|(1,\ 1+l)}, {}_2\tilde{k}^{1+l|(1,\ 1+l)}\right)$ of Sub. # $(1, 1 + l)$ $(l = 1, ..., 10)$ (10% noise in the first noise scenario)

$(i = n - 1, n)$, the substructures are simply denoted as Sub.#i $(i = 1, ..., n)$. Ten substructures can be generated from a 10-story building.

As Table 2 shows, a specific stiffness k_i can be estimated from Sub.#i-2 by using $({}_1\tilde{k}^{i|(i-2,i)}, {}_2\tilde{k}^{i|(i-2,i)})$ or from Sub.#i by using $({}_1\tilde{k}^{i|(i,i+2)}, {}_2\tilde{k}^{i|(i,i+2)})$ when these estimations have physical significance. The corresponding stiffness estimations are denoted below as $({}_1\tilde{k}^{i|i-2}, {}_2\tilde{k}^{i|i-2})$ and $({}_1\tilde{k}^{i|i}, {}_2\tilde{k}_{i|i})$.

3.2.1 | Accuracy of various stiffness estimations

First, the performance of the various estimates $\left({}_1\tilde{k}^{i|i-2}, {}_2\tilde{k}^{i|i-2}, {}_1\tilde{k}^{i|i}, {}_2\tilde{k}^{i|i}\right)$ was investigated for a specific stiffness k_i; Method 1 was used to solve for $({}_1\tilde{k}^{i|i-2}, {}_1\tilde{k}^{i|i})$, and Method 2 was used to solve for $\left({}_2\tilde{k}^{i|i-2}, {}_2\tilde{k}^{i|i}\right)$. Sub.#$i$-2 and Sub.#$i$ were used to estimate k_i.

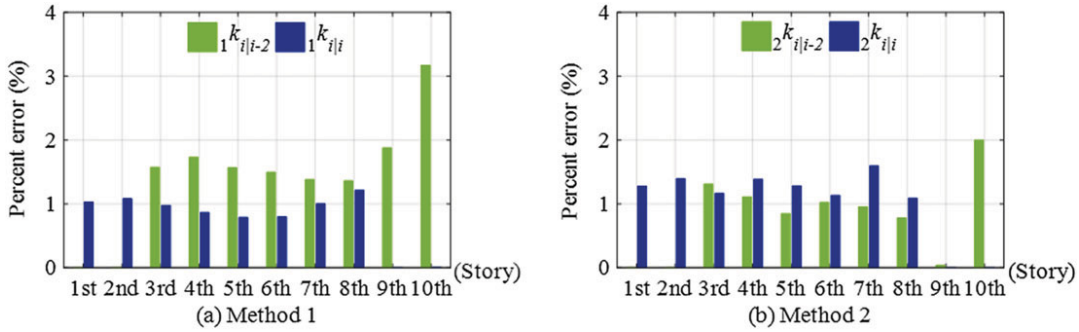

FIGURE 7 Percent error of $\left({}_1\tilde{k}^{i|i-2}, {}_1\tilde{k}^{i|i}, {}_2\tilde{k}^{i|i-2}, {}_2\tilde{k}^{i|i}\right)$ representing k_i (no noise)

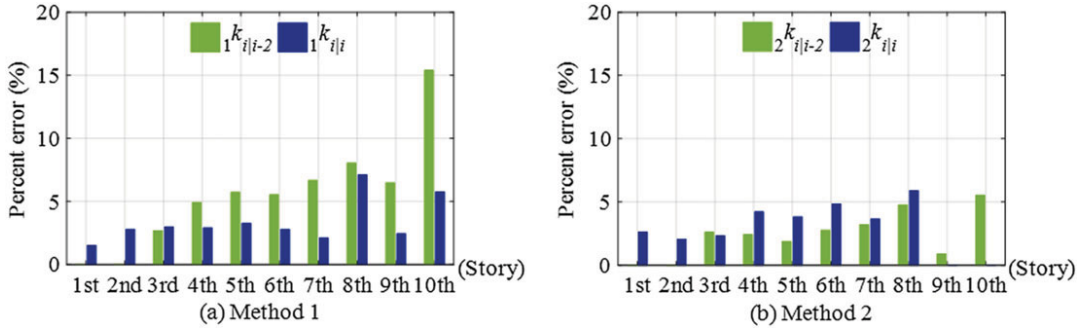

FIGURE 8 Percent error of $\left({}_1\tilde{k}^{i|i-2}, {}_1\tilde{k}^{i|i}, {}_2\tilde{k}^{i|i-2}, {}_2\tilde{k}^{i|i}\right)$ representing k_i (5% noise in the first noise scenario)

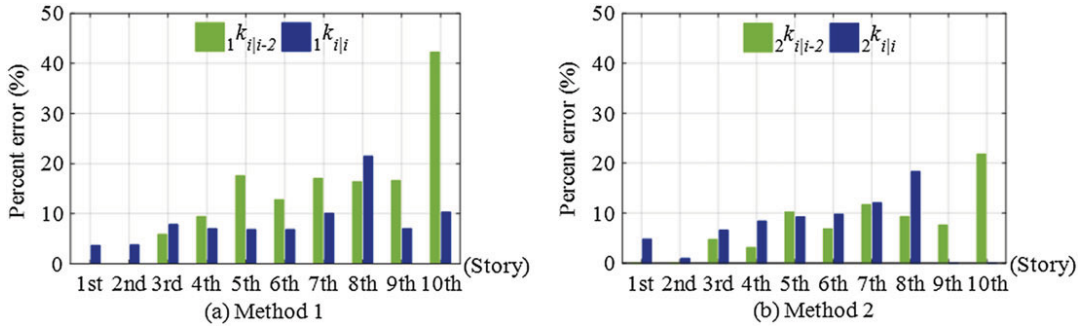

FIGURE 9 Percent error of $\left({}_1\widetilde{k}^{i|i-2}, {}_1\widetilde{k}^{i|i}, {}_2\widetilde{k}^{i|i-2}, {}_2\widetilde{k}^{i|i}\right)$ representing k_i (10% noise in the first noise scenario)

Figures 7–9 depict the percent errors of $\left({}_1\widetilde{k}^{i|i-2}, {}_1\widetilde{k}^{i|i}, {}_2\widetilde{k}^{i|i-2}, {}_2\widetilde{k}^{i|i}\right)$ (i is the story number) without noise and in the 5% and 10% noise cases of the first scenario. In Method 1, ${}_1\widetilde{k}^{i|i}$ of Sub.#i has comparatively higher accuracy than ${}_1\widetilde{k}^{i|i-2}$ of Sub.#i-2 at $i = 3, ..., 10$. In Method 2, ${}_2\widetilde{k}^{i|i-2}$ of Sub.#i-2 has comparatively higher accuracy than ${}_2\widetilde{k}^{i|i}$ of Sub.#i at $i = 3, ..., 8$. ${}_1\widetilde{k}^{i|i-2}$ and ${}_2\widetilde{k}^{i|i}$ were obtained from the linear relationship expressed in Equation 16. The premise of this equation is ($\delta = 0, \alpha = 0$) in Newmark's method, which may be the main reason for the above difference.

The average percent errors of Method 1 (${}_1\widetilde{k}_{i|i-2}, {}_1\widetilde{k}_{i|i}$) in Figures 7a–9a are (1.77%, 0.77%; no noise), (6.96%, 3.40%; 5% noise), and (17.52%, 8.49%; 10% noise). The average percent errors of Method 2 (${}_2\widetilde{k}_{i|i-2}, {}_2\widetilde{k}_{i|i}$) in Figures 7b–9b are (1.01%, 1.29%; no noise), (2.86%, 3.85%; 5% noise), and (10.37%, 9.15%; 10% noise). Overall, ${}_1\widetilde{k}_{i|i}$ of Method 1 is more accurate than the other three estimates, whereas the estimates of Method 2 are more robust to noise than those of Method 1.

${}_1\widetilde{k}_{i|i-2}$ and ${}_2\widetilde{k}_{i|i-2}$ have significantly larger errors at $i = 10$, corresponding to Sub.#8, whereas ${}_1\widetilde{k}^{i|i}$ and ${}_2\widetilde{k}^{i|i}$ have the maximum percent errors at Sub.#8 in the case of 10% noise. The probable reason is that Sub.#8, which is compromised of the top four floors, has a larger absolute noise effect compared with the other substructures, because in the first noise scenario, the noise intensity is proportional to the vibration intensity and the top floors vibrate more than the lower floors in the El Centro earthquake, whose major frequencies are close to the lower order natural frequencies of the building. To further illustrate this problem, the second noise scenario was simulated, where the noise intensity was the same for every measurement. As can be seen in Figures 10 (20% noise) and 11 (30% noise), the distributions of the percent errors are more even among the stories than in Figures 8 and 9.

Figures 7–11 show the linear relationship (Equation 16) among the coefficients of the ARMAX model, where ${}_1\widetilde{k}_{i|i-2}$ and ${}_2\widetilde{k}_{i|i}$ work effectively as ${}_1\widetilde{k}_{i|i}$ and ${}_2\widetilde{k}_{i|i-2}$, although there are some differences in the percent errors. Because $b_{21}(\cdot)$ in the ARMAX model (Equation 14; $i \le n - l$) is set to zero, the equation loses part of the input information. The stiffness of the system simulated with the ARMAX model is reduced as a result. This explains why the stiffness estimated from Subs.#i ($i \le n - 2, l = 2$) are generally smaller than the true value in the simulation.

3.2.2 | Stiffness identification of the whole building

The structural stiffness of the whole building can be identified in every substructure. A parallel calculation can be performed by analyzing at most four accelerations at a time. Because the stiffness of Subs.#i ($i \le n - 2$) are reduced by using

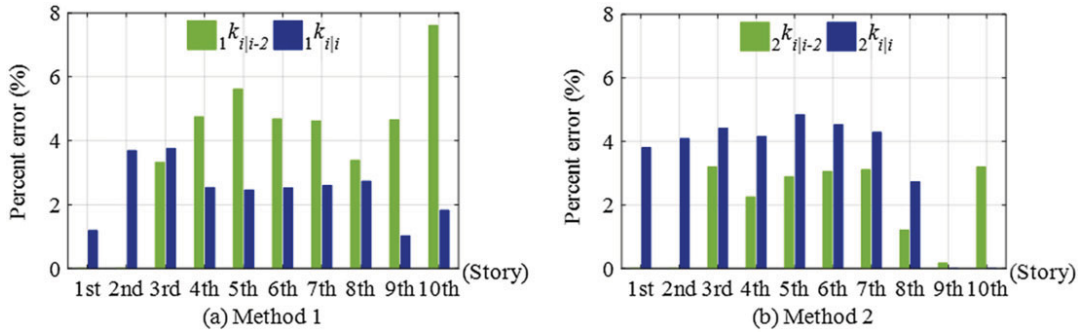

FIGURE 10 Percent error of $\left({}_1\widetilde{k}^{i|i-2}, {}_1\widetilde{k}^{i|i}, {}_2\widetilde{k}^{i|i-2}, {}_2\widetilde{k}^{i|i}\right)$ representing k_i (20% noise in the second noise scenario)

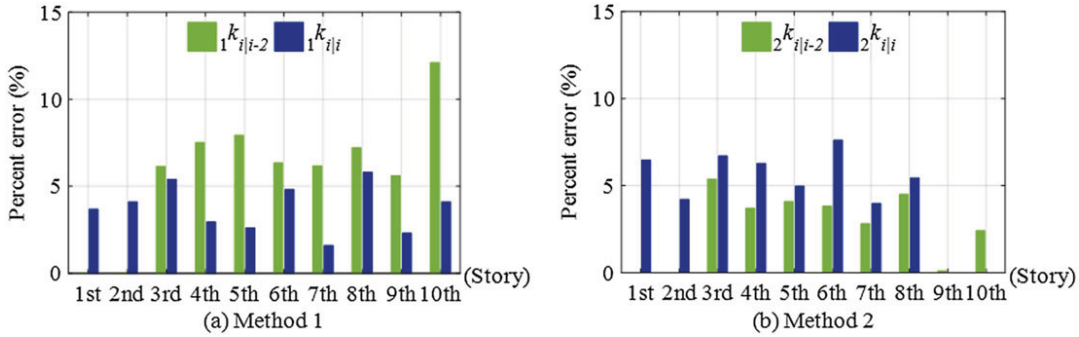

FIGURE 11 Percent error of $\left({}_1\widetilde{k}^{i|i-2}, {}_1\widetilde{k}^{i|i}, {}_2\widetilde{k}^{i|i-2}, {}_2\widetilde{k}^{i|i}\right)$ representing k_i (30% noise in the second noise scenario)

the ARMAX models, the best estimate of k_i ($i \le n-2$) should be the largest value of all possible estimates of k_i. For k_i ($i = n-1, n$), the best estimate could be $\widetilde{k}_{i|i}$, because the analysis in Section 3.2.1 shows that it is more accurate than the other estimates.

Figure 12 illustrates the substructure identification with an overlapping strategy. $\widetilde{k}_i$ is calculated as

$$\widetilde{k}_i = \begin{cases} \max\left({}_1\widetilde{k}_{i|i-2}\,{}_2\widetilde{k}_{i|i-2}\,{}_1\widetilde{k}_{i|i}\,{}_2\widetilde{k}_{i|i}\right), i = 1, \ldots, n-2; \\ {}_1\widetilde{k}_{i|i}, \qquad\qquad\qquad\qquad i = n-1, n. \end{cases} \tag{33}$$

where ${}_1\widetilde{k}_{i|i-2}$ and ${}_2\widetilde{k}_{i|i-2}$ are zero at $i = 1, 2$.

Substructure identification of the stiffness of the 10-story building (Figure 2) was simulated in first and second noise scenarios. As shown in Figures 13 and 14, all the structural stiffness are accurately estimated even in the cases of a large amount of noise. The percent errors of k_i in Figure 13 (the first scenario) are (0.00–1.08%; no noise), (1.52–5.76%; 5% noise), and (0.96–10.30%; 10% noise). In Figure 13 as in Figures 8 and 9, the percent errors are larger in the upper stories. The percent errors in Figure 14 (the second noise scenario) are more evenly distributed among the stories: (1.03–3.83%; 20% noise) and (1.59–5.37%; 30% noise).

3.3 | Comparison with previous substructure approach

The previous substructure approach proposed by Xing and Mita[19] and implemented in Mei et al.[20] was chosen for comparison. A concise description of their substructure approach is given here. For the n-story building depicted in Figure 1, n substructures are generated by taking out one story to form an SDOF system. The size of the substructure

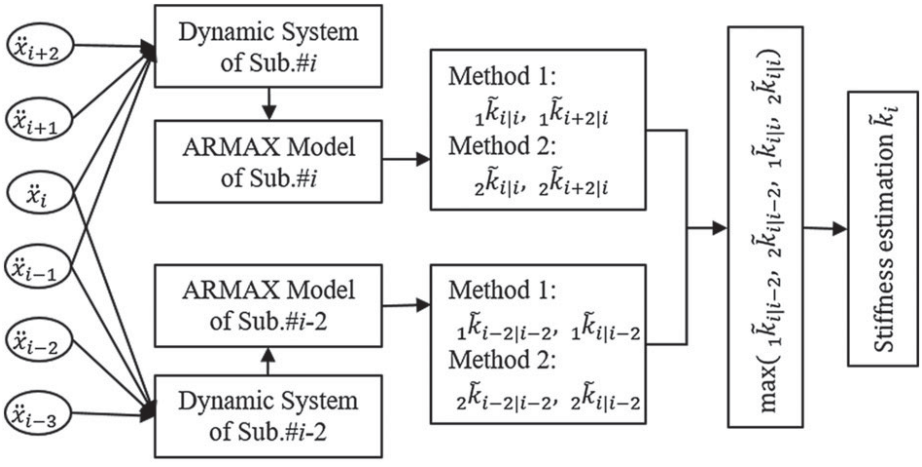

FIGURE 12 Stiffness estimation within substructure identification with overlapping strategy

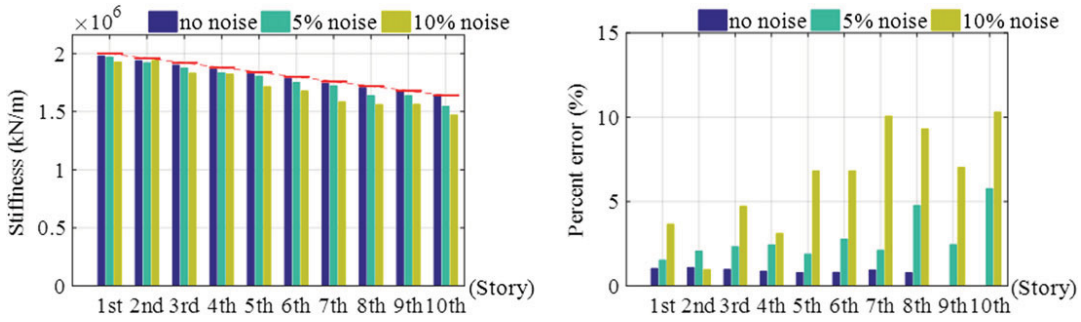

FIGURE 13 Estimated $\widetilde{k}_i$ and corresponding percent error (no noise, 5%, and 10% noise in the first noise scenario). The red solid line is the true value

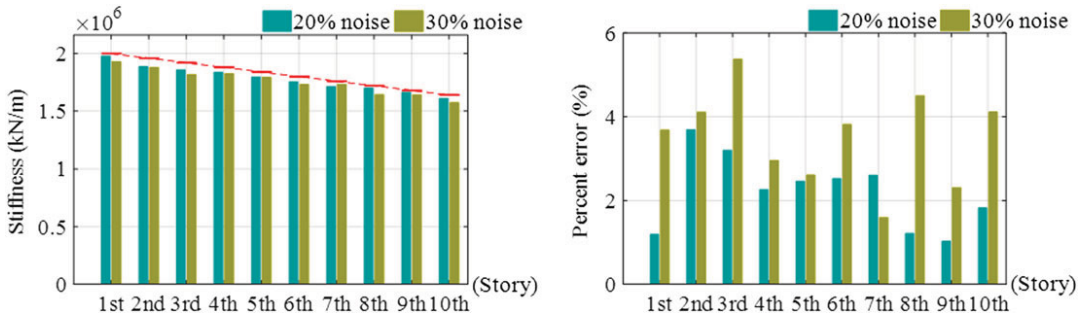

FIGURE 14 Estimated $\widetilde{k}_i$ and corresponding percent error (20% and 30% noise in the second noise scenario). The red solid line is the true value

is fixed to three floors. Let $c_{n+1} = 0$ and $k_{n+1} = 0$; the equation of motion of Sub.#i ($i = 1,..., n$, the story number) can be written as

$$m_i\ddot{y}_i(t) + (c_i + c_{i+1})\dot{y}_i(t) + (k_i + k_{i+1})y_i(t) = -m_i\ddot{x}_{i-1}(t) + c_{i+1}\dot{y}_{i+1}(t) + k_{i+1}y_{i+1}(t), i = 1, ..., n. \tag{34}$$

where $y_i(t)$ and $y_{i+1}(t)$ are the movements of m_i and m_{i+1} relative to m_{i-1} in Sub.#i ($i = 1, ..., n$). Central difference formulas are used to reformulate Equation 34 with accelerations. The following ARMAX model is obtained:

$$\begin{aligned}&\ddot{y}_i(t) + a_1\ddot{y}_i(t-1) + a_2\ddot{y}_i(t-2) = b_{11}\ddot{x}_{i-1}(t) + b_{12}\ddot{x}_{i-1}(t-1) + b_{13}\ddot{x}_{i-1}(t-2)\\ &+b_{21}\ddot{y}_{i+l}(t-1) + b_{22}\ddot{y}_{i+l}(t-2) + e(t) + g_1e(t-1) + g_2e(t-2), i = 1, ..., n.\end{aligned} \tag{35}$$

Stiffness identification was not the focus in the research presented in previous works,[19,20] so here, Equation 22 is used to extract the stiffness information from the ARMAX model (Equation 35). The stiffness combination ($k_i + k_{i+1}$) in Sub.#i (Equation 34) is able to be identified as follows:

$$\widetilde{k}_i + \widetilde{k}_{i+1} = m_i\left(\frac{|\ln\mu a|}{\Delta t}\right)^2, i = 1, ..., n, \tag{36}$$

where μa or μa^* defined in Equation 24 is the null point related with the coefficients of Equation 35. However, to obtain $\widetilde{k}_i$, all the above substructures including the ith story, that is, Subs.#i, ..., #n, need to be estimated.

Xing's substructure approach was then used to identify structural stiffness of the 10-story building (Figure 2) in the simulation. The noise levels of the first and second noise scenarios were the same as in Section 3.2.2. The percent errors of $\widetilde{k}_i$ in Figure 15 increase steeply with the noise level.

Compared with Figure 15, the percent errors in Figures 13 and 14 are much smaller and steadier at the same noise level. The proposed substructure approach has comparatively much better accuracy and robustness. Table 3 presents a detailed comparison with Xing's approach.

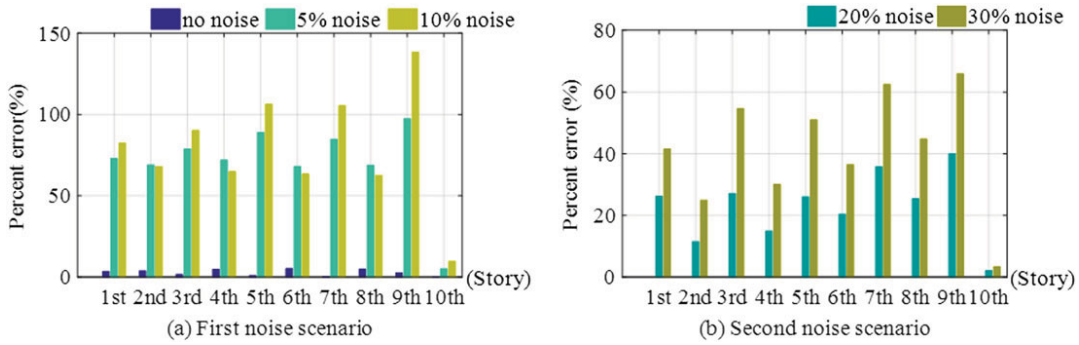

FIGURE 15 Percent error of $\widetilde{k}_i$ determined using previous substructure approach (no noise, 5%, and 10% noise in the first noise scenario (a); 20% and 30% noise in the second noise scenario (b))

TABLE 3 Comparison of the previous and proposed substructure approaches

	Previous substructure approach[17,18]	Proposed substructure approach
Size of substructure	a. Fixed, 3DOFs.	a. Arbitrary, suggested to be 4DOFs.
Substructure model	a. One model without further divisions; see Equation 34. b. No factor before m_i in Equation 34.	a. Further divided into two models: Method 1 (Equation 6) and Method 2 (Equation 26). b. $lm_i$and$lm_{i+l}$are used in Equations 6 and 26.
ARMAX model	a. Based on central difference formulas. b. No condensation (Equation 35).	a. Based on Newmark's method. b. Condensed (Equation 14).
Identifications	a. Stiffness combination $\widetilde{k}_i + \widetilde{k}_{i+1}$.	a. Individual stiffness: ${}_1\widetilde{k}_{i\|(i,i+l)}$, ${}_1\widetilde{k}_{i+l\|(i,i+l)}$, ${}_2\widetilde{k}_{i\|(i,i+l)}$, ${}_2\widetilde{k}_{i+l\|(i,i+l)}$.
Performance	a. Works well without noise; no robust to noise. b. Need Subs.#i, ..., #n to identify $\widetilde{k}_i$. c. Distributed monitoring is difficult.	a. Works well even when there is large amount of noise: Very robust. b. $\widetilde{k}_i$ can be identified from Sub.#i-2 or Sub.#i. c. Distributed monitoring is possible.

Note. ARMAX = autoregressive-moving average with exogenous; DOFs = degrees of freedom.

4 | SHAKING-TABLE EXPERIMENT

Because the effect of the noise is very difficult to model precisely in the simulation, it becomes vital to conduct an actual experiment for testing the substructure approach. Here, a shaking-table experiment of a five-story three-dimensional frame, as shown in Figure 16a, was carried out at the Mita Laboratory of Keio University. Six accelerometers were used to monitor the vibrations of the structure and shaking table; one was installed on each floor (including the basement).

The floor of the frame was an aluminum slab and four bronze columns (plates) were attached it. The theoretical stiffness of each column was calculated from its size by using Young's modulus of bronze (1.0×10^{11} N/m^2). The size and weak-axis stiffness of the plates are shown in Figure 16b. The positions of the columns are shown in Figure 16c. Some plates (Type 1) were 2.5 mm thick; the others (Type 2) were 1.5 mm thick. Two columns on the second story and one column on the fifth story were Type 2; the other columns were Type 1. The mass of the frame was in the aluminum slabs, bronze columns and accelerometers, and the stiffness of the frame was the sum of the four columns. Table 4 lists the structural mass and stiffness information. The global modal frequencies of the frame were 2.40, 7.45, 11.16, 13.55, and 16.47 Hz for the first to fifth mode.

A sinusoidal wave with a major frequency around 3.7 Hz was used as the input signal. The acceleration time histories were sampled at 200 Hz. The structure started to vibrate about 10 s after the start of sampling. The acceleration records used in the analysis were 5-s long with 1,000 points and sampled after 10-s vibration. There were five substructures in the analysis: Sub.#(i, $i+2$) ($i = 1, 2, 3$) and Sub.#(i, $n+1$) ($i = 4,5$).

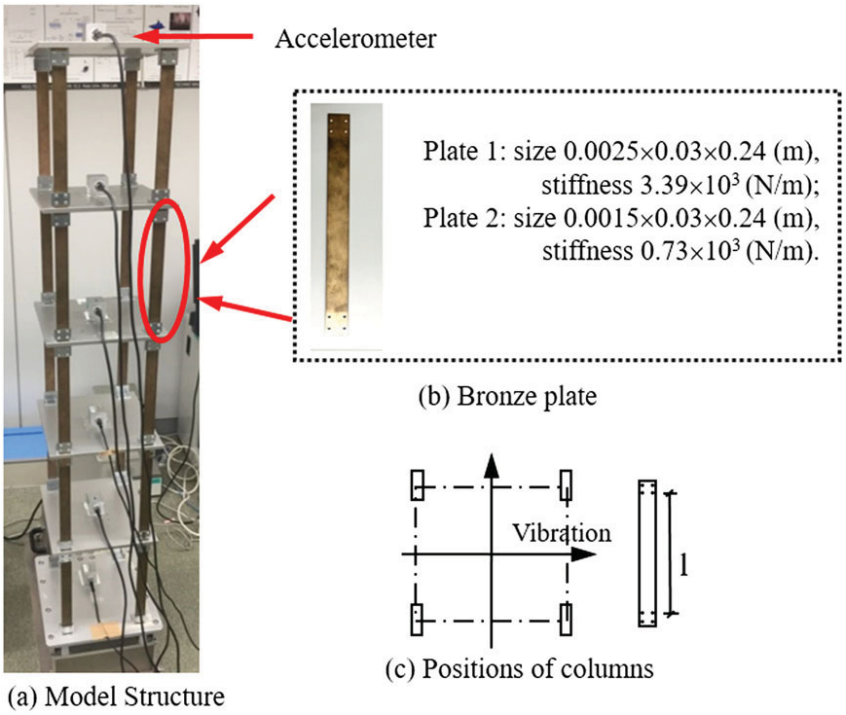

FIGURE 16 Five-story frame structure in the Mita Laboratory

TABLE 4 Theoretical mass and stiffness of five-story frame

Property	1st story	Second story	Third story	Fourth story	Fifth story
Mass (kg)	4.25	4.25	4.36	4.31	3.49
Stiffness (kN/m)	13.56	8.25	13.56	13.56	10.90

4.1 | Stiffness estimation among substructures

First, the accuracies of the stiffness estimates $({}_1\widetilde{k}_{i|i-2}, {}_2\widetilde{k}_{i|i-2})$ from Sub.#i-2 and $({}_1\widetilde{k}_{i|i}, {}_2\widetilde{k}_{i|i})$ from Sub.#i were examined. These were representative values for k_i $(i = 1, 2, 3, 4, 5)$. As in Table 2, $({}_1\widetilde{k}_{i|i-2}, {}_1\widetilde{k}_{i|i})$ were the results of Method 1 and $({}_2\widetilde{k}_{i|i-2}, {}_2\widetilde{k}_{i|i})$ were the results of Method 2.

The identification of $({}_1\widetilde{k}_{i|i-2}, {}_1\widetilde{k}_{i|i}, {}_2\widetilde{k}_{i|i-2}, {}_2\widetilde{k}_{i|i})$ and percent errors at $i = 1, 2, 3, 4, 5$ are presented in Figures 17 and 18, where the theoretical stiffness is from Table 4. The substructure approach can correctly estimate every stiffness of $({}_1\widetilde{k}_{i|i-2}, {}_1\widetilde{k}_{i|i}, {}_2\widetilde{k}_{i|i-2}, {}_2\widetilde{k}_{i|i})$. All the stiffness identifications are very close to the theoretical value. Similar to the conclusions obtained in Section 3.2.1, most stiffness identifications are close to or less than the theoretical value. The percent errors of Method 1 are 0.52–13.20%, whereas those of Method 2 are 0.98–11.53%. The average errors of ${}_1\widetilde{k}_{i|i-2}, {}_1\widetilde{k}_{i|i}, {}_2\widetilde{k}_{i|i-2}$ and ${}_2\widetilde{k}_{i|i}$ are 7.40%, 2.36%, 4.09%, and 6.55%, respectively.

4.2 | Stiffness identification of the whole structure at different sampling frequencies

The substructure identification with overlapping (Figure 12) and Equation 33 were used to estimate the whole structural stiffness $\widetilde{k}_i (i = 1, 2, 3, 4, 5)$ of the five-story building in the experiment. Many earthquake records have been made by sampling at lower frequencies, that is, 100 and 50 Hz. For this reason, structural stiffness identifications were conducted at these frequencies as well. In this case, resampling was used to lower the sampling frequency of the acceleration measurements. The length of the data in the analysis was 1,000 points.

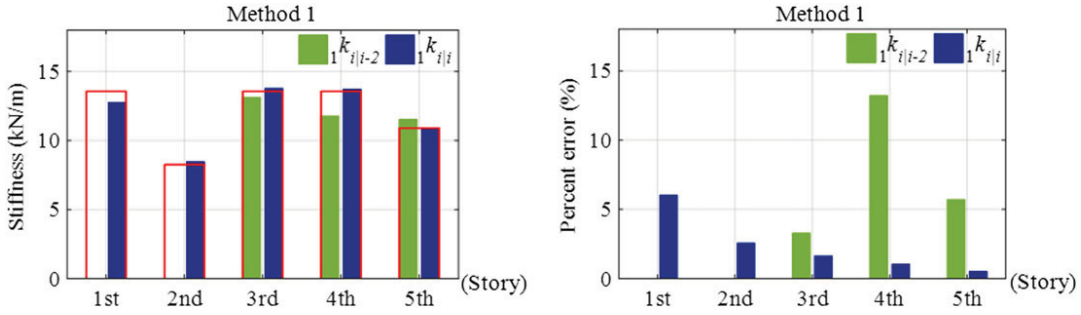

FIGURE 17 Identified substructure parameters $({}_1\widetilde{k}_{i|i-2}, {}_1\widetilde{k}_{i|i})$ of Method 1 and their percent errors in the experiment test. The red edged bars indicate the theoretical stiffness

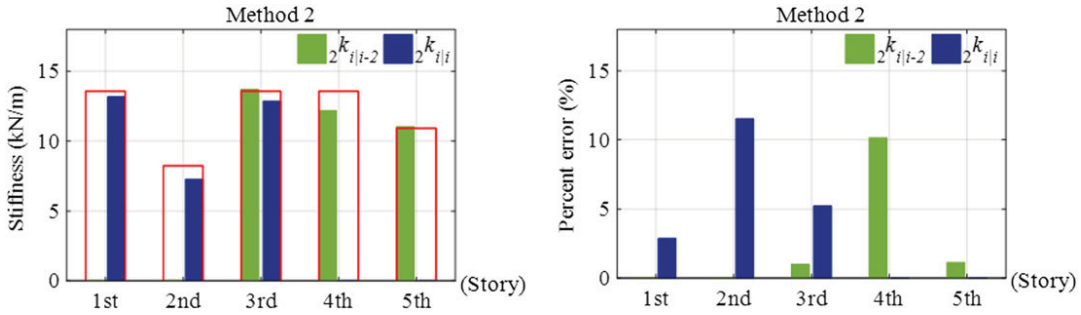

FIGURE 18 Identified substructure parameters $({}_2\widetilde{k}_{i|i-2}, {}_2\widetilde{k}_{i|i})$ of Method 2 and their percent errors in the experiment. The red edged bars indicate the theoretical stiffness

As shown in Figure 19, $\widetilde{k}_i (i = 1,\ 2,\ 3,\ 4,\ 5)$ can all be identified accurately at sampling frequencies of 200, 100, and 50 Hz. The percent errors of $\widetilde{k}_i (i = 1,\ 2,\ 3,\ 4,\ 5)$ are 0.52–2.88% (200 Hz), 0.64–6.99% (100 Hz), and 1.94–5.19% (50 Hz). The results obtained for 200 Hz are slightly more accurate than those of 100 and 50 Hz.

4.3 | Structural identification verification without theoretical values

In most situations, the theoretical stiffness of a building is very difficult to calculate. A popular way of assessing the effectiveness of a structural parameter identification is to simulate the system output of the identified structural model for a given input and see if it matches the measured output.

The structural model of the five-story building in the experiment was reconstructed by using the identified $\widetilde{k}_i (i = 1,\ 2,\ 3,\ 4,\ 5)$ at a sampling frequency of 200 Hz (Figure 19) and by assuming the following damping ratios of each s: $\widetilde{\zeta}_i = 0.018\ (i = 1,\ 2,\ 3,\ 4,\ 5)$. The equations of motion of the whole structure (Equation 1) can be rewritten as

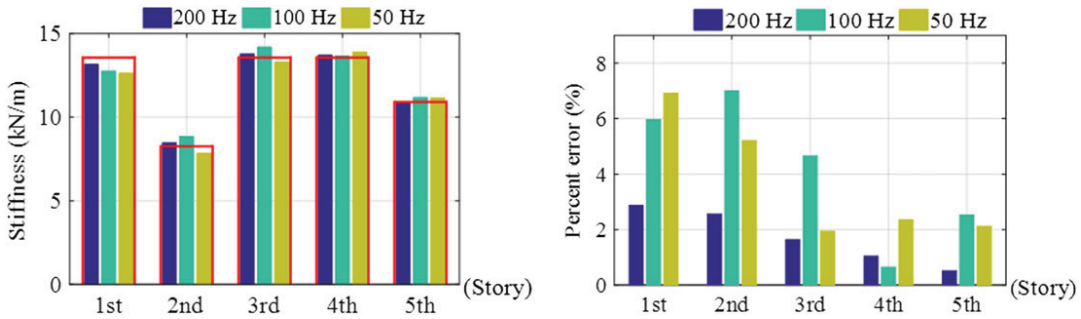

FIGURE 19 Estimated $\widetilde{k}_i$ and corresponding percent errors in the experiment at different sampling frequencies: (200, 100, and 50 Hz). The red edged bars indicate the theoretical stiffness

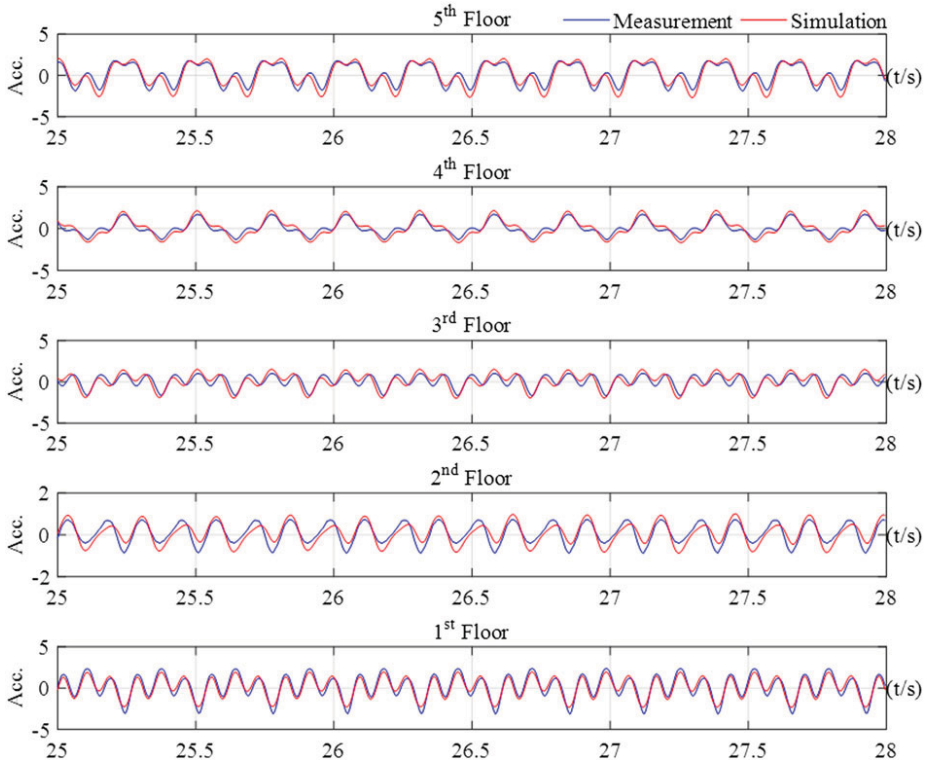

FIGURE 20 Comparison of simulated and measured structural accelerations

$$\mathbf{M}\ddot{\mathbf{z}}(t) + \widetilde{\mathbf{C}}\dot{\mathbf{z}}(t) + \widetilde{\mathbf{K}}\mathbf{z}(t) = -\mathbf{ML}\ddot{x}_g(t), \tag{37}$$

where $\widetilde{\mathbf{C}}$ and $\widetilde{\mathbf{K}}$ are the estimated damping matrix and stiffness matrix composed of $\widetilde{c}_i$ and $\widetilde{k}_i$, respectively. $\widetilde{c}_i$ is calculated as

$$\widetilde{c}_i = 2\widetilde{\zeta}_i\sqrt{m_i\widetilde{k}_i}, (i = 1,\ 2,\ 3,\ 4,\ 5). \tag{38}$$

Because $\widetilde{c}_i$ and $\widetilde{k}_i$ can be normalized by dividing by m_i, Equation 37 does not require any detailed information on m_i. The input signal $\ddot{x}_g(t)$ consists of the measurements of the shaking-table experiment.

Solving Equation 37 by using the state-space method reproduces the structural accelerations, as depicted in Figure 20. The shape and amplitude of the simulated acceleration of every floor are very close to those of the measured acceleration. These results demonstrate the effectiveness of the structural parameter identification even without theoretical values.

5 | CONCLUSIONS

The new substructure approach provides a fast and effective way to separately identify structural parameters of any part of a shear structure from SDOF substructure models formed using Method 1 or Method 2. Parallel parameter identification in every substructure can be performed by processing at most four accelerometers. The numerical simulation showed that the new approach can deal with large amounts of noise (5% noise in the first scenario and 30% noise in the second scenario) with less than 5% errors in the stiffness estimation of most substructures. The shaking-table experiment indicated that the errors are less than 3% at a sampling frequency of 200 Hz, and the simulated structural accelerations of the identified structural model matched the measurements. Compared with previous methods, the new method has much greater versatility, accuracy, and robustness.

ACKNOWLEDGEMENTS

The financial support from the Japanese Government (Monbukagakusho: MEXT) Scholarship and the GESL (Global Environmental System Leaders) Program of Keio University is gratefully acknowledged.

ORCID

Lijun Xie http://orcid.org/0000-0002-3618-8549
Longxi Luo http://orcid.org/0000-0003-2661-4177

REFERENCES

[1] P. C. Chang, A. Flatau, S. C. Liu, *Struct. Health Monit.* **2003**, *2*(3), 257.

[2] H. Sun, R. Betti, *Struct. Control Health Monit.* **2014**, *21*(6), 868.

[3] S. Mukhopadhyay, H. Lus, R. Betti, *Struct. Control Health Monit.* **2015**, *22*(7), 1024.

[4] C. A. Perez-Ramirez, J. P. Amezquita-Sanchez, H. Adeli, M. Valtierra-Rodriguez, D. Camarena-Martinez, R. J. Romero-Troncoso, *Eng. Appl. Artif. Intel.* **2016**, *48*, 1.

[5] S. W. Doebling, C. R. Farrar, M. B. Prime, D. W. Shevitz. Damage identification and health monitoring of structural and mechanical systems from changes in their vibration characteristics: a literature review. Technical Report LA-13070-MS, Los Alamos National Laboratory, Los Alamos, NM, **1996**.

[6] C. G. Koh, L. M. See, T. Balendra, *Earthq. Eng. Struct. Dyn.* **1991**, *20*(8), 787.

[7] C. G. Koh, B. Hong, C. Y. Liaw, *Eng. Struct.* **2003**, *25*(12), 1551.

[8] C. G. Koh, K. Shankar, *J. Eng. Mech.* **2003**, *129*(7), 769.

[9] K. V. Yuen, L. S. Katafygiotis, *Comput. Aided Civ. Inf. Eng.* **2006**, *21*(4), 280.

[10] K. F. Tee, C. G. Koh, S. T. Quek, *Struct. Health Monit.* **2009**, *8*(5), 397.

[11] J. Hou, Ł. Jankowski, J. Ou, *Struct. Control Health Monit.* **2011**, *18*(6), 601.

[12] J. Hou, Ł. Jankowski, J. Ou, *Struct. Control Health Monit.* **2012**, *19*(4), 491.

[13] D. Zhang, E. A. Johnson, *Smart Mater. Struct.* **2012**, *21*(5), 055006.

[14] A. W. Oreta, T. A. Tanabe, *Doboku Gakkai Ronbunshu* **1993**, *1993*(459), 19.

[15] K. F. Tee, C. G. Koh, S. T. Quek, *Earthq. Eng. Struct. Dyn.* **2005**, *34*(15), 1755.

[16] C. B. Yun, H. J. Lee, *Struct. Saf.* **1997**, *19*(1), 121.

[17] Q. Zhao, T. Sawada, K. Hirao, Y. Nariyuki, *Earthq. Eng. Struct. Dyn.* **1995**, *24*(3), 325.

[18] A. Mita. Distributed health monitoring system for a tall building. *In Proceedings of 2nd International Workshop on Structural Control* **1996**: 333–340.

[19] Z. Xing, A. A. Mita, *Struct. Control Health Monit.* **2012**, *19*(2), 309.

[20] L. Mei, A. Mita, J. Zhou, *Struct. Control Health Monit.* **2016**, *23*(2), 218.

[21] A. K. Chopra, *Dynamics of structures*, Prentice Hall, Englewood, Cliffs, NJ **1995**.

[22] C. G. Lee, C. B. Yun, *Comput. Struct.* **1991**, *40*(6), 1475.

How to cite this article: Xie L, Mita A, Luo L, Feng MQ. Innovative substructure approach to estimating structural parameters of shear structures. *Struct Control Health Monit*. 2018;25:e2139. https://doi.org/10.1002/stc.2139